Transactions of the Materials Research Society of Japan 33[4] 1073-1076 (2008)

Compositional and Valence state Inhomogeneities in $Ce_{1-x}Tb_xO_{2-\delta}$ ($0.10 \leq x \leq 0.70$)

Fei Ye, Toshiyuki Mori, Ding Rong Ou, Jin Zou* and John Drennan*
Fuel Cell Materials Center, National Institute for Materials Science, 1-1 Namiki, Tsukuba, Ibaraki 305-0044, Japan
Fax: 81-29-860-4667, e-mail: fei.ye@nims.go.jp
*Centre for Microscopy and Microanalysis, The University of Queensland, St Lucia, Brisbane, Qld 4072 Australia

Compositional and valence state inhomogeneities were confirmed in $Ce_{1-x}Tb_xO_{2-\delta}$ ($0.10 \leq x \leq 0.70$) sintered samples by electron energy-loss spectroscopy (EELS) and energy-filtering transmission electron microscopy (EFTEM). It was found that both Tb and Ce cations have mixed valence (trivalence and tetravalence). Through EFTEM study, nano-domains with higher Tb concentration than the matrix were observed. Furthermore, by using a novel method based on EFTEM, the valence state maps were achieved, showing that both Ce^{3+} and Tb^{3+} cations tend to segregate into the domains.
Key words: Microstructure, Conductivity, TEM, Domain

1. INTRODUCTION

Ceria based oxides have been widely used as three-way catalysts,[1,2] oxygen permeation membranes,[3] oxygen gas sensors,[4] fuel cell electrolytes and electrodes.[5] Among these doped ceria materials, Tb-doped ceria presents electrical properties of mixed conductors (electronic and ionic), which can be of interest for their potential use as electrodes for intermediate temperature fuel cells and for oxygen membranes.[6] Furthermore, Tb-doped ceria has attracted increasing attentions because it has shown advantage in the performance of three-way catalysts.[7-11] Comparing with other trivalent dopants (e.g. Y^{3+}, Gd^{3+}), Tb was confirmed to have mixed valence of Tb^{3+} and Tb^{4+} in Tb-doped ceria by X-ray absorption near edge structure (XANES),[6,12] which can contribute to the mixed conduction as well as the catalytic and redox properties.

Recently, nano-sized domains in numerous ceria doped with trivalent dopant have been observed using high resolution transmission electron microscopy (HRTEM).[13-19] These domains can have negative impacts on the electrical conductivity of doped ceria. A study of energy-filtering transmission electron microscopy (EFTEM) indicated that the dopant cations could segregate into the domains.[19] However, the microstructure at nano-scale was seldom studied in Tb-doped ceria. Furthermore, because Tb has mixed valence, not only the compositional but also valence state characteristics can have significant influence on the electrical properties of Tb-doped ceria. Therefore, the study of these characteristics is desired for the purpose of applications.

For these reasons, in the present work, the microstructures in $Ce_{1-x}Tb_xO_{2-\delta}$ ($0.10 \leq x \leq 0.70$) sintered samples, especially the distributions of composition and valence state, are studied by using EFTEM and electron energy-loss spectroscopy (EELS). Usually, EFTEM is used for the observation of the compositional distribution. In this work, a novel method based on EFTEM is developed to obtain valence state maps, from which the relative distribution of valence state can be clearly shown. Then the relationship between the compositional and valence state distributions and the formation of the domains were analyzed.

2. EXPERIMENTAL

Highly dense $Ce_{1-x}Tb_xO_{2-\delta}$ ($0.1 \leq x \leq 0.7$) sintered samples were prepared from the nano-powders synthesized via the ammonium carbonate coprecipitation method reported elsewhere.[20] The powders were isostatically pressed under 200 MPa pressure. Then the compacted bodies were heated to 1400°C at a rate of 5°C/min. After holding for 6h, the samples were cooled to room temperature at a rate of 5°C/min.

The microstructures of the sintered samples were identified by X-ray diffraction (XRD, RINT2200HF) and TEM. To prepare TEM samples, small discs with a diameter of 3 mm were cut from the sintered samples by ultrasonic cutter. Then the thickness of the discs was reduced orderly by mechanical grinding, dimpling and ion milling. HRTEM observation was performed in a JEOL JEM-2000EX TEM. EFTEM and EELS were performed in a Philips Tecnai G^2 F30 TEM equipped with a Gatan Imaging Filtering system. Both EFTEM and EELS observations were carried on in specimens that were sufficiently thin and deviated away from the strong Bragg condition.

3. RESULTS

The distributions of composition are first studied by EFTEM. Because of the high intensity of Ce and Tb N edges, the EFTEM elemental maps of Ce and Tb were obtained by using the N edges with an energy window of 10 eV opened on the edges. Then the darker point on the Ce or Tb maps can indicates a lower concentration of Ce or Tb.

Besides the usual EFTEM elemental maps, in this work, valence state map can be achieved by using a novel method based on EFTEM. The principle of this method is based on the characteristics of the EELS $M_{4,5}$ edge of lanthanides. Fig. 1 shows the $M_{4,5}$ edges of Ce and Tb in the sample with $x = 0.50$, which is taken from a large area in the sample corresponding to the average

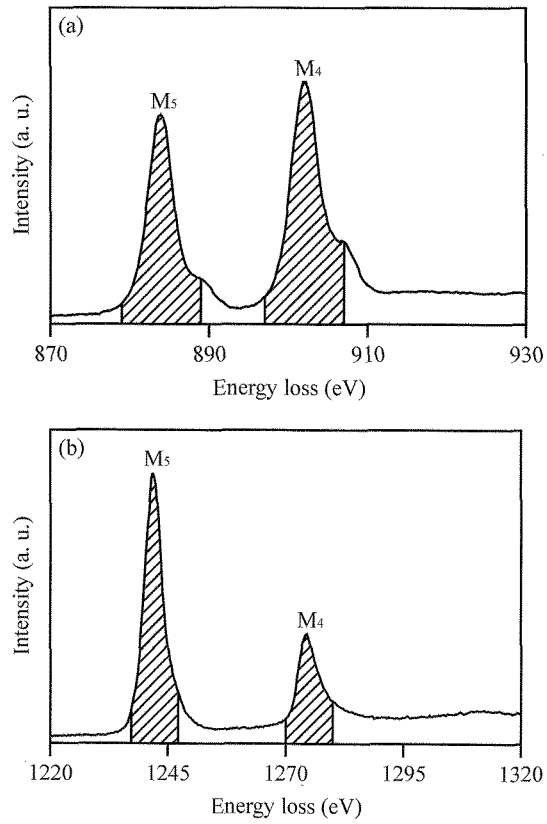

Fig. 1. EELS spectra of (a) Ce and (b) Tb $M_{4,5}$ edges taken from a large area in $Ce_{0.5}Tb_{0.5}O_{2-\delta}$ corresponding to the average composition. I(M4)/I(M5) values of Ce and Tb are 1.17 and 0.39, respectively. The shadow areas indicate the energy windows to obtain valence state maps of EFTEM.

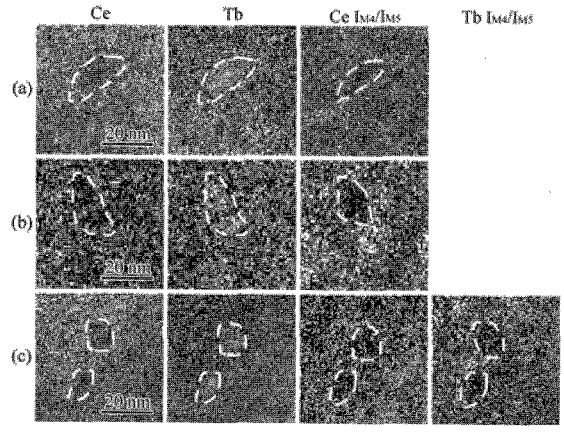

Fig. 2. Elemental and valence state maps of Ce and Tb. (a) $Ce_{0.9}Tb_{0.1}O_{2-\delta}$, (b) $Ce_{0.5}Tb_{0.5}O_{2-\delta}$, (c) $Ce_{0.3}Tb_{0.7}O_{2-\delta}$.

composition. The sharp M_4 and M_5 peaks arise from the spin-orbit splitting of the 3d initial states and their relative intensity is a reflection of the 4f final state orbital, and hence the valence.[21-24] The decrease in the values of I(M4)/I(M5) is related to the increase in trivalent cation concentration. For example, in Fig. 1, the I(M4)/I(M5) values of Ce and Tb are 1.17 and 0.39 respectively. It was reported the I(M4)/I(M5) value of Ce for CeO_2 is 1.25, which is larger than that shown in Fig. 1. Therefore, Ce has mixed valence state of Ce^{3+} and Ce^{4+} in this sample. Based on this principle, it is possible to achieve valence state maps by using the following method. Firstly, EFTEM maps were obtained by using M_4 and M_5 peaks, respectively, with energy windows of 10 eV opened on the peaks as indicated by shadows in Fig. 1. Then the valence state map is constructed by dividing the map of M_4 peak by the map of M_5 peak. In other words, the valence state map is constructed according to the relative intensities of the corresponding points on the maps of M_4 and M_5 peaks. The relative intensities are calculated by I_{M4}/I_{M5}, where I_{M4} and I_{M5} are intensities of the corresponding points on the maps of M_4 and M_5 peaks. Thus, a darker point in the valence state map of Ce or Tb indicates a lower value of I_{M4}/I_{M5} and thereby a higher concentration of Ce^{3+} or Tb^{3+} cations.

EFTEM elemental and valence state maps of $Ce_{1-x}Tb_xO_{2-\delta}$ samples are shown in Fig. 2. When $x \le 0.5$, the Tb $M_{4,5}$ edges are too weak to obtain a clear Tb valence state map, so that only the Tb valence state map of $Ce_{0.3}Tb_{0.7}O_{2-\delta}$ is shown in Fig. 2. As can be seen in Fig. 2, both the composition and the valence state of Ce and Tb are inhomogeneous. Some dark areas in Ce map with a size between 10–20 nm, as roughly enclosed by dashed lines, become white in Tb map, indicating these areas are corresponding to the aggregates of Tb cations. Furthermore, these areas are darker in the valence state map of Ce and Tb, while the sizes are a bit different from those in the elemental maps. As aforementioned, the dark point is related with the increase in trivalent cation concentration. Therefore, it can be concluded that these aggregates of Tb are companied by the aggregation of trivalent cations.

The compositional and valence state inhomogeneities can be further confirmed by EELS. In $Ce_{0.5}Tb_{0.5}O_{2-\delta}$, the Tb concentration of an aggregate of Tb was measured to be 52 at.%. Simultaneously, the Tb concentration of the surrounding matrix is decreased to about 43 at.%. The actual compositional difference between the aggregates and the matrix may be larger, because the size of the aggregates is only several nanometers and the observed aggregates may be embedded in the matrix. Furthermore, as mentioned above, the value of $I(M_4)/I(M_5)$ is a source of valence state information. For this reason, the ionic valence in the aggregates and matrix of the sample with $x = 0.50$ was qualitatively characterized using Ce and Tb $M_{4,5}$ edges. Fig. 3 shows the EELS spectra of Ce and Tb $M_{4,5}$ edges that were normalized with respect to the intensities of M_4 edges. The $I(M_4)/I(M_5)$ values of Ce are 0.85 and 1.12 for the aggregates and matrix respectively, which are smaller than the value of 1.25 for CeO_2,[24] indicating that Ce also has mixed valence as Tb in Tb-doped ceria. Additionally, it can be seen that the I(M4)/I(M5)) values of Ce and Tb of the aggregates (0.85 and 0.37, respectively) are both smaller than those of the matrix (1.12 and 0.41, respectively), which suggests that both Ce^{3+} and Tb^{3+}cations could segregate into the aggregates. These results are well consistent with those shown in Fig. 2.

To find out the correspondence between the microstructure and the compositional and valence state inhomogeneity, the microstructure of the samples were

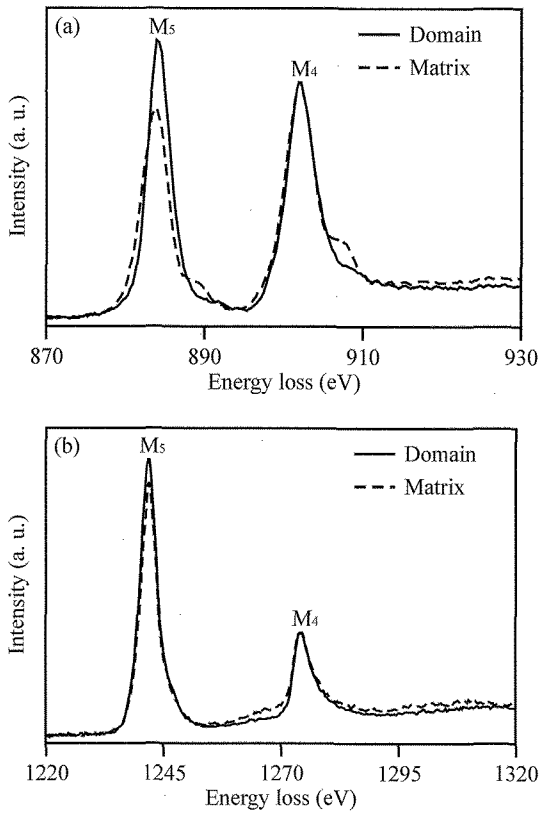

Fig. 3. EELS spectra of (a) Ce and (b) Tb $M_{4,5}$ edges taken from the aggregates (domains) and the matrix in $Ce_{0.5}Tb_{0.5}O_{2-\delta}$. I(M4)/I(M5) values of Ce are 0.85 and 1.12 for the domains and the matrix, respectively; and those of Tb are 0.37 and 0.41, respectively.

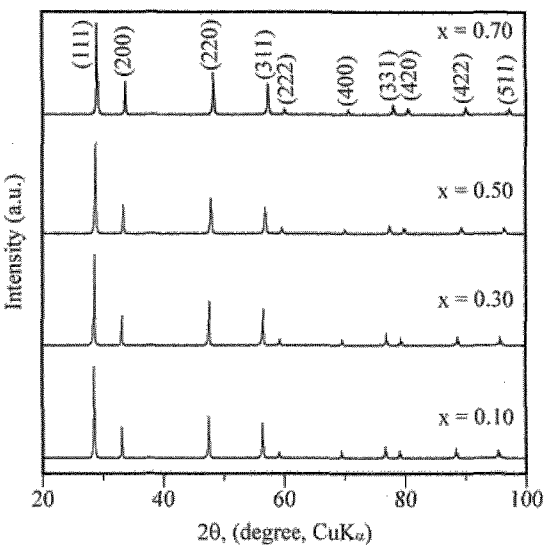

Fig. 4. XRD profiles of sintered samples.

then studied by XRD and HRTEM. Fig. 4 is the XRD profiles, showing that the Tb-doped ceria samples consist of simple fluorite structure. This result shows that Tb has much higher solubility in ceria than other types of dopant. For example, the solubility of yttrium-doped ceria is about 35 at.% at 1500°C.

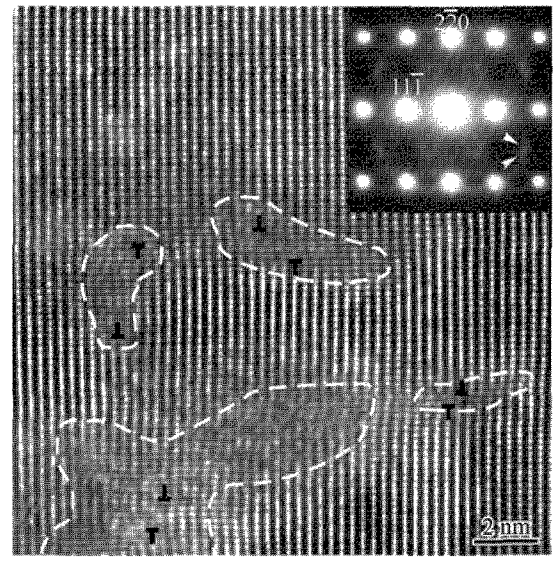

Fig. 5. [112] HRTEM image of $Ce_{0.5}Tb_{0.5}O_{2-\delta}$. The inset is the corresponding SAED pattern.

However, since XRD deals with a large volume of a sample, it is insensitive to the small deviation of the microstructure. For this reason, the detailed microstructure needs to be further examined by TEM. It is found that the compositional and valence state inhomogeneities are accompanied by a microstructural inhomogeneity. As in other types of doped ceria, nano-sized domains can also be observed.[13-19] Fig. 5 shows the [112] HRTEM image of the $Ce_{0.5}Tb_{0.5}O_{2-\delta}$, on which some nano-sized domains with lattice distortion could be seen as roughly enclosed by dashed lines. Half atomic planes marked by "T" are observed in/around the domains in the figure. The size of the domains shown in the figure is about 2 – 10 nm. Moreover, in the corresponding selected area electron diffraction (SAED) pattern in Fig. 5, periodic extra reflections (as indicated by arrows) and diffuse scattering can be seen between the reflections of the fluorite structure. These extra reflections and diffuse scattering are related to the domains, which indicate that the domains tend to have an ordered structure. HRTEM study shows that these domains can be observed in the samples with different Tb concentrations, while their density and size increase with increasing the Tb concentration. By comparing the HRTEM observation with Fig. 2, we believe that the nano-sized domains in Fig. 4 are corresponding to the aggregates in Fig. 5.

4. DISCUSSION

The mixed valence of Tb confirmed by EELS and EFTEM is consistent with the study of XANES.[6,12] However, Ce cations have mixed valence in the present work, which is inconsistent with the full oxidized state that determined by the XANES study.[12] We suspect that this difference is possibly related to the preparation methods of the samples. Furthermore, besides the mixed valence of Tb and Ce, the compositional and valence state inhomogeneities were observed in this work. Tb, especially Tb^{3+} cations, prefers segregation into the nano-sized domains. These domains with the

aggregation of dopant cations had been observed in Y-doped ceria.[19] However, in Tb-doped ceria, Ce^{3+} cations also segregate into the domains although the concentration of Ce in the domains is lower than that of the matrix, which has never been reported in other rare-earth-doped ceria.

The reason for the inhomogeneities of the composition, valence state and microstructure remains unclear. We suspect that one possibility is related to the defect clustering. In doped ceria, it was suggest that the oxygen vacancies will aggregate into clusters in dilute range.[26,27] Hence the trivalent cations (i.e. mainly Tb^{3+}, and Ce^{3+} in this study), as its charge compensator, are attracted by the clusters due to Coulomb interactions and the requirement of electrical neutrality of the cluster. The aforementioned clustering of dopant cations and oxygen vacancies can be supported by atomistic simulations.[28,29] As the doping concentration increase, the clusters may grow larger, which could lead to the compositional and valence state inhomogeneities and in turn the microstructural inhomogeneity observed in the present work.

5. CONCLUSIONS

The compositional and valence state inhomogeneities were observed in Tb-doped ceria for the first time through studies of EELS and EFTEM, which are accompanied by the microstructural inhomogeneity, i.e. the formation of the nano-sized domains. Valence state maps were obtained by a new approach based on EFTEM. It was observed that the Tb concentration in the domains is higher than the matrix. Furthermore, Tb^{3+} and Ce^{3+} cations could segregate into the domains. Such inhomogeneities in composition and valence state are related to the defect clustering. They might be one of the driving forces for the formation of the domains.

REFERENCES

[1] J. Kašpar, P. Fornasiero and M. Graziani, *Catal. Today*, **50**, 285-98 (1999).
[2] A. Trovarelli, "Catalysis by Ceria and Related Materials", Imperial College Press, London, (2002).
[3] M. Stoukides, *Catal. Rev. Sci. Eng.*, **42**, 1-70 (2000).
[4] N. Izu, W. Shin, I. Matsubara and N. Murayama, *J. Electroceram.*, **13**, 703-06 (2004).
[5] B. C. H. Steele, *Solid State Ionics*, **134**, 3-20 (2000).
[6] P. Shuk, M. Greenblatt and M. Croft, *Chem. Mater.*, **11**, 473-79 (1999).
[7] F. Zamar, A. Trovarelli, C. de Leitenburg and G. Dolcetti, *Stud. Surf. Sci. Catal.*, **101**, 128392 (1996).
[8] S. Bernal, G. Blanco, M. A. Cauqui, P. Corchado, J. M. Pintado and J. M. Rodríguez-Izquierdo, *Chem. Commun.*, 1545-46 (1997).
[9] S. Bernal, G. Blanco, M. A. Cauqui, M. P. Corchado, C. Larese, J. M. Pintado and J. M. Rodríguez-Izquierdo, *Catal. Today*, **53**, 607-12 (1999).
[10] G. Blanco, J. J. Calvino, M. A. Cauqui, P. Corchado, C. López-Cartes, C. Colliex, J. A. Pérez-Omil and O. Stephan, *Chem. Mater.*, **11**, 3610-19 (1999).
[11] A. B. Hungría, A. Martínez-Arias, M. Fernández-García, A. Iglesias-Juez, A. Guerrero-Ruiz, J. J. Calvino, J. C. Conesa and J. Soria, *Chem. Mater.*, **15**, 4309-16 (2003).
[12] X. Wang, J. C. Hanson, G. Liu, J. A. Rodriguez, A. Iglesias-Juez and M. Fernández-García, *J. Chem. Phys.*, **121**, 5434-44 (2004).
[13] T. Mori, J. Drennan, Y. Wang, J. H. Lee, J. G. Li and T. Ikegami, *J. Electrochem. Soc.*, **150**, A665-73 (2003).
[14] T. Mori, J. Drennan, J. H. Lee, J. G. Li and T. Ikegami, *Solid State Ionics*, **154-155**, 461-66 (2002).
[15] T. Mori, Y. Wang, J. Drennan, G. Auchterlonie, J. G. Li, T. Ikegami, *Solid State Ionics*, **175**, 641-49 (2004).
[16] T. Mori, T. Kobayashi, Y. Wang, J. Drennan, T. Nishimura, J. G. Li and H. Kobayashi, *J. Am. Ceram. Soc.*, **88**, 1981-84 (2005).
[17] T. Mori, J. Drennan, Y. Wang, G. Auchterlonie, J. G. Li and A. Yago, *Sci. Technol. Adv. Mater.*, **4**, 213-20 (2003).
[18] D. R. Ou, T. Mori, F. Ye, J. Zou and J. Drennan, *Acta Mater.*, **54**, 3737-46 (2006).
[19] D. R. Ou, T. Mori, F. Ye, J. Zou, G. Auchterlonie and J. Drennan, *Electrochem. Solid-State Lett.*, **10**, P1-3 (2007).
[20] F. Ye, T. Mori, D.R. Ou, R. Buchanan, J. Zou and J. Drennan, *J. Nanosci. Nanotechnol.*, **7**, 2521-25 (2007).
[21] T. Manoubi and C. Colliex, *J. Phys. Chem. Solids*, **50**, 1 (1990).
[22] B. T. Thole, G. van der Laan, J. C. Fuggle, G. A. Sawatzky, R. C. Karnatak and J.-M. Esteva, *Phys. Rev. B*, **32**, 5107-18 (1985).
[23] L. A. J. Garvie and P. R. Buseck, *J. Phys. Chem. Solids*, **60**, 1943-47 (1999).
[24] S. Arai, S. Muto, J. Murai, T. Sasaki, Y. Ukyo, K. Kuroda and H. Saka, *Mater. Trans.*, **45**, 2951-55 (2004).
[25] V. Longo and L. Podda, *J. Mater. Sci.*, **16**, 839-41 (1981).
[26] C. R. A. Catlow, "Nonstoichiometric Oxides", Ed. by O. Toft Sørensen, Academic Press, Lodon (1981) pp. 61-99.
[27] D. Y. Wang, D. S. Park, J. Griffith and A. S. Nowick, *Solid State Ionics*, **2**, 95-105 (1981).
[28] L. Minervini, M. O. Zacate and R. W. Grimes, *Solid State Ionics*, **116**, 339-49 (1999).
[29] H. Inaba, R. Sagawa, H. Hayashi and K. Kawamura, *Solid State Ionics*, **122**, 95-103 (1999).

(Recieved December 9, 2007 ; Accepted September 1, 2008)